OCEAN DIGEST

Quarterly Newsletter of the Ocean Society of India

Volume 8 | Issue 2 | April 2021 | ISSN 2394-1928

Detection of Generation Location and Phase Speed of Internal Solitary Waves in the Andaman Sea using Multiple Satellite Observations



Mihir Kumar Dash[1], Jithendra Raju Nadimpalli[2] and Chinglen Meetei Tensubam[3]

[1]Centre for Oceans, Rivers, Atmosphere and Land Sciences (CORAL), Indian Institute of Technology Kharagpur, INDIA
[2]Department of Aerospace Engineering, Indian Institute of Technology Madras, INDIA
[3]Department of Infrastructure Engineering, The University of Melbourne, AUSTRALIA

1.0 Introduction

Internal waves are non-linear gravity waves formed in a stratified, rotating ocean attributed to the disturbances that formed at the density interfaces. High tidal flow over a steep topography, continental shelf can induce large-scale disturbances at the pycnocline and lead to the formation of internal solitary waves (ISWs or solitary waves hereafter) (Shimizu and Nakayama 2017). ISW can induce vertical mass transport and vertical mixing and hence play a vital role in enhancing biological production by affecting the exchange of heat, nutrients, and other properties (Alford et al. 2015). They can influence acoustic propagation and are proven hazard to offshore oil and gas drilling platforms. The crests and troughs associated with mode-1 (first baroclinic mode) ISW traveling along the pycnocline can create zones of divergence and convergence patterns at the ocean surface. These surface manifestations exhibit a distinctive pattern on the ocean surface roughness that is observed as alternative bright/dark bands in both Synthetic Aperture Rader (SAR) and true-colour sunglint imagery due to enhanced/reduced backscatter. Important ISW parameters like amplitude, wavelength, crest length, width of solitons, number of waves per packet, inter packet distances, and direction of propagation can be determined from these surface signatures captured in the satellite images (Jackson 2009; Liu et al. 2014b). A suitable combination of image pairs captured by various satellite sensors, the phase speed of ISWs can be estimated (Liu et al. 2014a, 2014b; Yang et al. 2014).

The shallow sills located between islands, steep continental slopes, stratification by freshwater addition from the Irrawaddy river and high tidal velocities make the Andaman Sea (hereafter abbreviated as AnS) an attractive location for the study of ISWs. Several studies using satellite and in-situ observations reveal different generation sites of ISWs in the Andaman Sea (Magalhaes and da Silva 2018; Alpers et al. 1997; Jackson 2004). Using syntheticaperture radar (SAR) observations, Alpers et al. (1997) noted that shallow banks or presence of sea-mounts in the AnS are the potential sites of solitary waves. Magalhaes and da Silva (2018) showed that both mode-1 and mode-2 internal solitary waves are present in the 10° channel in the AnS and propagate towards east. Employing the moored buoy data. Another interesting study by Wijeratne et al. (2010) speculated that large-amplitude seiches observed along the east coast of Sri Lanka can be excited by ISW, which originates in the Nicobar Islands and propagates to the Sri Lankan coast in 6–8 days. Most of the studies on ISWs in AnS using both moored buoy and satellite imagery are concentrated mostly on the vertical structure, influence, and propagation.

The article describes the Generation locations and propagation characteristics of ISWs in the Andaman Sea using multi-satellite images. With multiple hotspots and frequent occurrence of ISWs, the Andaman Sea is an ideal place to analyze the propagation speed of ISWs by comparing multiple satellite images. Furthermore, availability of SAR and sunglint optical images from different remote sensing platforms enables comprehensive analysis of ISWs in this region.

2.0 Generation locations of ISWs in the Andaman region as observed from MODIS true-colour images

Wider swath (2300 km), high spatial resolution (250 m), and better geolocation accuracy (about 60 m) make the true-colour images of Moderate Resolution Imaging Spectroradiometer (MODIS) an ideal sensor to investigate the ISWs (Jackson 2007). The detection of ISWs in MODIS images is limited by sun-satellite geometry (sunglint area), the cloud cover and (Jackson et al. 2012). High cloud cover in South-West and North East monsoon and tropical cyclones formed in the Bay of Bengal during the pre- and post-monsoon periods restrict ocean observation in the optical wavelengths. However, calm weather during February, March, and April provide an opportunity to acquire cloud-free satellite imagery over the AnS. Moreover, in February, the position of the sun and the satellites (Terra and Aqua) at these latitudes are not coherent to produce bright sunglint region. Therefore, the sunglint imagery of MODIS for the months of March and April in the years 2014–2016 is considered in this study. ISWs manifest themselves as packet of waves propagating away from the generation site in the satellite image. In the close vicinity of generation site, ISW manifests itself as distorted arcs in packets and propagating outward. Figure-1 shows the MODIS true colour images capturing 6 ISWs in the southern AnS. As evidenced from the curvature of wavefronts in a wave packet, the potential generation site appears somewhere in the close vicinity of the great passage and waves that radially propagate towards east after being generated on subsequent phases of the tide. As the leading wavefront scatters more energy towards the satellite receiver compared with other tail waves, spotting the leading wave is relatively easy.

All the MODIS sunglint images in the month of March and April during 2014 to 2016 are analysed and the curvature of leading wavefront for each wave packet is delineated, and a composite map is prepared (see Fig. 2). In total 312 mode-1 ISW packets were observed during this period. To determine the circumcentre of each wavefront in a wave packet, the interface of leading crest and trough is identified and manually mapped in ArcGIS environment. Circumcentre is computed using the first, middle, and last points on the leading wavefront. Then, the position of the circumcentre is optimised using least square fit technique considering all the points on the arc. The circumcentre coordinates of all such similar wavefronts are averaged to obtain the possible generation location of corresponding ISW. As shown in Fig. 2, the ISWs are radiating after being generated from five locations, labelled in the alphabetical order from A to E. The ISWs from A, B, and E appear to be propagating in a

single direction while those at C and D show signatures of wave propagation in two opposite directions.

ISWs from A propagate in the southwest direction onto the continental shelf of the eastern part of Andaman Islands. ISWs from B travel towards the northeast of AnS and onto the continental shelf of Myanmar. During propagation, they interact with the shelf present to the north of direction of propagation and modified into a shape of 'number 7' instead of a circular curvature that is commonly seen in the world oceans. This modified shape is maintained until it encounters the long continental shelf (Fig. 2). However, the ISWs generated at C travel along both east and west directions (Fig. 2). The westward waves traverse towards the southern Bay of Bengal, while the eastward waves headed for the shelf of Myanmar and Thailand. Those generated at the west of D travel in the southwest direction towards the southern Bay of Bengal while those formed at the east of D appear to be refracted towards northeast just after their generation. During the propagation, they cut across ISWs generated from C and propagate without any further changes in the direction. However, during the study period, their surface signatures are not visible after crossing the waves generated at C. The ISWs generated at E travel to the east along the shallow shelf of Malacca Strait and Thailand. The crest lines of these wave packets spread from 5° N to 9° N latitudes over the continental shelf of south-eastern AnS. They cross paths with the ISWs generated at C obliquely and form 'X' shaped patterns.

3.0 Determination of phase velocity of ISWs in the Andaman using multi satellite observations

Images captured by six instruments from five different satellite missions are used to detect and study ISWs in the Andaman Sea. Suitable combination of SAR images of EnviSat and ERS–2 (tandem satellites), optical sunglint images of MODIS onboard Terra and Aqua, Medium Resolution Imaging Spectrometer (MERIS) onboard EnviSat, and Visible Infrared Imaging Radiometer Suite (VIIRS) onboard Suomi National Polar-orbiting Partnership Satellite are used to compute the phase speeds of ISWs. The main advantages of SAR sensors are high spatial resolution and all-weather sensing capabilities to observe the earth surface. However, low temporal resolution and narrow swath width are the limitations of SAR images. On the other hand, optical sensors such as MODIS, MERIS and VIIRS have wide swaths which can scan the entire basin and capture trains of ISW packets at a snapshot. These optical sensors also have high temporal coverage, which increases the imaging frequency. The surface signatures of ISWs are readily detected in sunglint and cloud free regions of these optical imageries. However, sensing by optical remote sensing is greatly affected by the presence of cloud cover, especially during the monsoon and post-monsoon months (June to October) over this region. Therefore, most of cloud free sunglint images over this region are available in March, April and May months and same have been used for ISWs detection and analysis along with other images. It is to be noted that contrast enhancement is performed in all optical images to make ISWs distinctly detectable. All the ISWs presented in this study are taken in the years 2002, 2004, 2007, 2008, 2010, 2015 and 2016.

All the images are downloaded from public domain. Each image pixel contains either backscattering or reflected radiance values from the ocean surface along with its geographic information. The images are then projected using a World Geodetic System (WGS) 1984 Universal Transverse Mercator (UTM) Zone 46 N in the ArcGIS environment. Generally, mode-1 ISWs are visible as pattern of bright bands followed by dark bands in SAR images (Jackson et al. 2012). However, in sunglint optical images, the same waves are visible as a pattern of dark bands followed by bright bands (Jackson 2007). Each wave

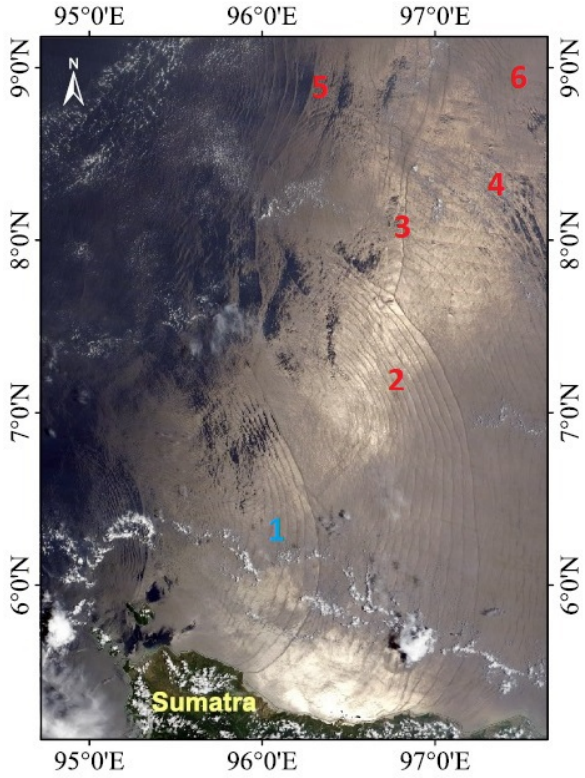

Figure 1: ISWs in the southern Andaman Sea propagating towards continental shelf of Thailand captured by MODIS true-colour image on 22 March 2015 (adopted from Raju et al. 2019)

packet in the image consists of a leading wavefront followed by a trailing wave train. The amplitude of the Bragg waves is increased (decreased) at the convergence (divergence) zone created by the internal waves. Thus, the surface roughness is enhanced in convergence region and decreases in the divergence zone. The rough convergence (smooth divergence) zone appears to be bright (dark) in SAR imagery, whereas reverse case is observed in sunglint optical images (Alpers et al. 2008). The geolocations of the leading wavefront(s) of ISW packet(s) is (are) traced by taking the central pixels of bright (dark) patches in SAR (sunglint optical) image for the entire study period. A total of 426 ISW packets are detected from the images captured by different sensors during the study period.

The estimation of phase speed of ISWs require a pair of images which captures the same packet within a small time interval. 11 such image pairs are selected with suitable combination. Each image pair is represented by alphabets from A–K and is shown in Fig.3. The ISW(s) present in each image pair is (are) numbered using a numeric value. For example: 'B1' represents 1st ISW present in image pair 'B'. The composite of all 11 image pairs is shown in Fig. 3(L).

3.1. Multiple Images Comparison (MIC) method to derive the phase speed

One or more ISW packets can be observed by two different sensors subsequently with some time gap between their observations. For example, MODIS-Aqua on 16*th* January 2010 captured two ISW packets propagating in the northeast direction towards the Thailand coast. Approximately, 200 *min*. ago, the same packets were captured by EnviSat ASAR. In order to compute the phase speed, the images in a image-pair are

georeferenced and projected to WGS-1984 UTM Zone 46 N in the ArcGIS environment. The wavefronts of each packet are then traced by taking geolocations of the central pixels of bright (in SAR images) or dark (in sunglint optical images) stripes in the projected images. Since the horizontal resolution of the images are different, to measure the displacement of the wavefront, the geolocation points on two wavefronts are considered and not the pixel size of the image. Similarly, for the remaining image pairs, the leading wavefronts of all ISW packets contained in the image pairs are traced. Transects are then drawn normal to both the projected leading wavefronts, and the lengths of these transects give the displacements by the ISWs within the time interval of the image pairs. There are navigational errors of half apixel approximately in the construction of wavefronts. This can add some error to the calculation of the phase velocity depending on time interval between two observations. For example, there is an error of125 *m* for a pixel size of 250 *m* in the MODIS image. An ISW packet with typical phase speed of 2.20 *m/s* can propagate a distance of 7.92 *km* between time interval that a pair of satellites capture the waves, say 60*min*. for EnviSat and MODIS. Then, 125 *m* navigational error will affect the ISW phase speed estimation by about 1.60%. The maximum errors that can be incorporated to the calculation of phase speed ranges from 0.74-5.50% depending on the spatial resolution of image and time interval between two satellite passes. Figure 3 shows a composite picture of displacements at different points of the leading wavefronts of the 24 ISWs observed in the 11 image pairs. As we can see from Figure 3(i) that a wavefront displaces unequal distances at the different locations. In other words, it means a wavefront propagates at different phase speeds at different locations/depths. The minimum, maximum and average phase speeds of a wavefront are calculated from its displacements divided by time interval between the two sensors capturing the wavefront. We called this method as Multiple Images Comparison (MIC) method. The estimated average ISW phase speeds are indicate that the phase speed of ISWs in south-easternpart of Andaman Sea varies between 1.59 to 2.47 m/s, whereas phase speed to be from 1.68 to 2.74 m/ s in the east-central part. In region surrounding Nicobar and east of Andaman Islands, the ISW phase speed varies between 2.15 to 2.76 m/s and 1.75 to 2.55 m/s respectively . One of the causes for the variation of the phase speed in a region is the bathymetry of the region. And other cause could be the variation in the thickness of stratified layer present in the region.

4.0 Summary

The generation region and phase speed of ISWs in the Andaman Sea is studied using images obtained from Active and Passive satellite sensors. A total of 426 ISW packets are detected using six different satellite instruments (SAR, ASAR-WSM, MERIS, MODIS-Aqua, MODIS-Terra and VIIRS) during December 2002 and May 2016.It is observed that ISWs are ubiquitous in the AnS. The study reveals that there are five hotspots of mode-1long living ISWs. One is located at the shelf break of northeast AnS and the remaining four are identified along the passages joining Myanmar, North Andaman Island; Car Nicobar, Chowra Island of Nicobar Islands, Teressa Island and Katchal Island of Nicobar Islands, and Great Nicobar Island, Northern

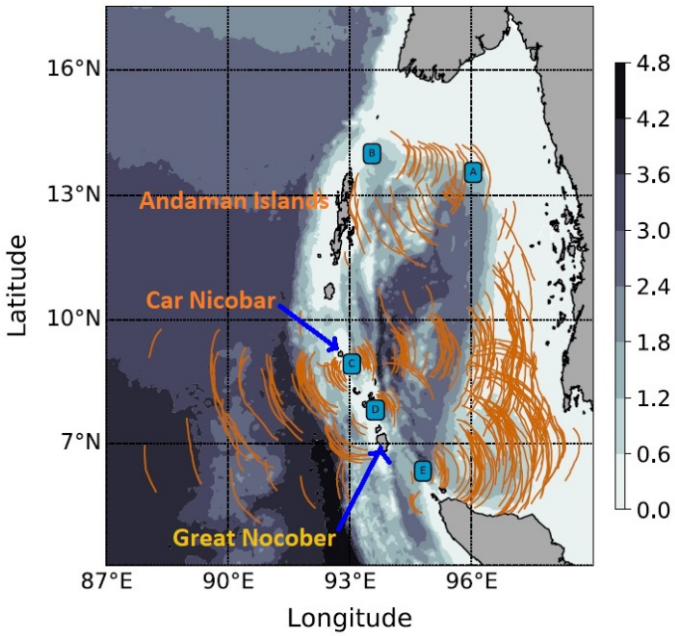

Figure 2: Leading waves in each solitary wave packet observed in the MODIS images during the months of March and April from 2014 through 2016. Blue boxes with alphabets denote the possible generation sites of these ISWs. The shading shows depth in kilometres (Adopted from Raju et al., 2019)

Sumatra, respectively. Generation sites between the Nicobar Islands radiate ISWs in both directions depending on phase of the tidal flow. Among the images analyzed, 11 SAR and sunglint optical image pairs are used to estimate the phase speed of 24 ISWs in the Andaman Sea. The estimated phase speeds vary between 1.59 to 2.76 m/s. Finally, this study shows that satellite images can effectively be used to estimate ISW phase speed, which is one of the important ISW parameter to understand generation, dispersion and its dissipation.

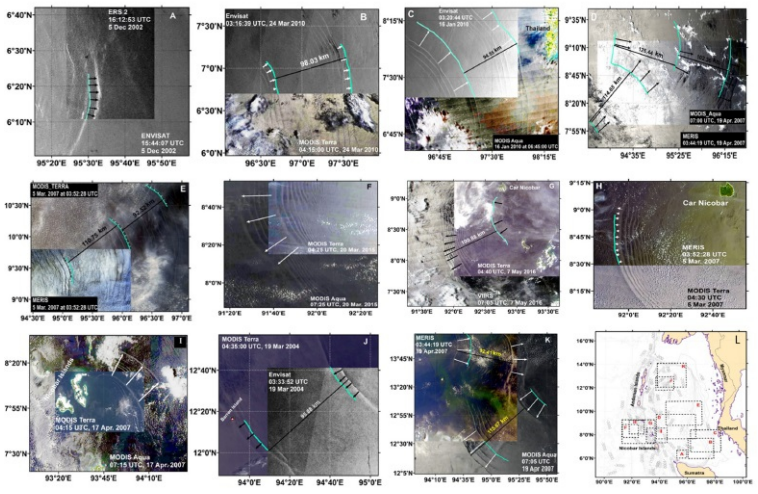

Fig. 3. *11 image pairs capturing propagation of 24 ISWs at different regions of the Andaman Sea. Green curves are the projected leading wavefronts of ISW packets overlaid by another image of the pair. The black and white arrows represent ISW propagation directions. The straight thick black lines are the interpacket distances. The map (L) shows the location of these 11 image pairs in the Andaman Sea (Meetei et al., 2021).*

References:

Alford, M.H., Thomas, P., Jennifer, A.M.,Jonathan, D.N., Maarten, C.B., Luca, R.C. et al. (2015): The formation and fate of internal waves in the South China Sea, Nature, 521, 65–69.

Alpers, W., Brandt, P., Rubino, A. (2008): Internal waves generated in

the Straits of Gibraltar and Messina: Observations from Space, Remote sensing of the European seas, Springer, pp. 319–330.
Alpers, W., Wang-Chen, H., & Hock, L. (1997): Observation of internal waves in the Andaman Sea by ERS SAR, In Geoscience and Remote Sensing, 1997, IGARSS'97. Remote Sensing-A Scientific Vision for Sustainable Development., 1997 IEEE International (Vol. 4, pp. 1518–1520).
Jackson, C. R., Da Silva, J. C. B., & Jeans, G. (2012): The generation of nonlinear internal waves, Oceanography, 25.
Jackson, C.R. (2009): An empirical model for estimating the geographic location of nonlinear internal solitary waves, Journal of Atmospheric and Oceanic Technology, 26, 2243–2255.
Jackson, C. (2007): Internal wave detection using the moderate resolution imaging spectroradiometer (MODIS), Journal of Geophysical Research: Oceans, 112(C11).
Jackson, C. R. (2004): An atlas of internal solitary-like waves and their properties.
Liu, B., Yang, H., Ding, X., Li, X., (2014a): Tracking the internal waves in the South China Sea with environmental satellite sun glint images, Remote sensing letters, 5, 609–618.
Liu, B., Yang, H., Zhao, Z., Li, X., (2014b): Internal solitary wave propagation observed by tandem satellites, Geophysical Research Letters, 41, 2077–2085.
Magalhaes, J. M., & da Silva, J. (2018): Internal solitary waves in the Andaman Sea : new insights from SAR imagery. Remote Sensing, 10(6), 861.
Meetei T. Chinglen , N. J. Raju, Mihir K. Dash and H. Barskar (2021): Estimation of internal solitary wave propagation speed in the Andaman Sea using multi–satellite images, Remote sensing of the environment, 252,
Raju N. J., Mihir K. Dash, Subhra Prakash Dey and Prasad K. Bhaskaran (2019): Potential generation sites of internal solitary waves and their propagation characteristics in the Andaman Sea—a study based on MODIS true-colour and SAR observations, Environ Monit. Assess. 191(Suppl 3): 809.
Shimizu, K., and Nakayama, K. (2017): Effects of topography and Earth's rotation on the oblique interaction of internal solitary like waves in the Andaman Sea, Journal of Geophysical Research: Oceans, 122(9), 7449–7465.
Wijeratne, E. M. S., Woodworth, P. L., & Pugh, D. T. (2010): Meteorological and internal wave forcing of seiches along the Sri Lanka coast, Journal of Geophysical Research, 115(C3), C03014.
Yang, H., Liu, B., Zhao, Z., Li, X., (2014): Inferring internal wave phase speed from multi-satellite observations. In: Geoscience and Remote Sensing Symposium (IGARSS), 2014 IEEE International, IEEE, pp. 4768–4771.

Response of the Atmospheric Boundary Layer in the Air-Sea Interaction Processes: A Historical Perspective

D. Bala Subrahamanyam
Space Physics Laboratory, Vikram Sarabhai Space Centre
Department of Space, Government of India,
Indian Space Research Organisation
Thiruvananthapuram – 695022, Kerala, India
E-mail: subrahamanyam@gmail.com
Tel: +91-9895656150; Fax: +91-471-2706535

The atmospheric boundary layer (ABL), also known as the planetary boundary layer (PBL) is defined as the lowest part of the Earth's atmosphere which is directly influenced by the presence of the earth's surface in which the effects of the surface forcings (frictional drag, evaporation and transpiration, heat transfer, pollutant emission, and terrain induced flow modifications) are felt directly on a timescale less than a day (Stull 1988; Garratt 1992). The importance of this layer becomes more crucial when we deal with the ocean-land-atmosphere interaction processes as a significant flux of momentum, heat or matter are carried by turbulent motions on a scale of the order of the depth of the ABL or less. Most of the solar radiation is absorbed in the ground and is transmitted back to the rest of the atmosphere by ABL processes. Quantitatively, almost half of the atmospheric kinetic energy is dissipated in ABL. Our current understanding about the ABL processes is an outcome of a comprehensive, consistent and concerted efforts of several top-class researchers in the past. The present article is a trivial attempt to revisit the journey of scientific research that led to the recognition of ABL as one of the pioneering areas in the area of atmospheric and oceanic sciences, and eventually provided a strong foundation for dedicated theoretical investigations for understanding the air-sea interaction processes.

The concept of the boundary layer (BL) can not be considered as a discovery, as it remained a part and parcel of the fluid dynamics discipline ever since the conceptualization of a fluid flow in a scientific manner. We can find a piece of credible evidence about our understanding of the interaction of a fluid with a solid from the ancient times of Archimedes (287 - 212 BC), who was a Greek mathematician and mechanical engineer, a pioneer in both fields, many centuries ahead of his contemporaries. Archimedes had formally put forward his principle, also known as the law of buoyance which states that any object fully or partially immersed in a fluid will experience an upward force equal to the weight of the displaced fluid. This discovery was an outcome of a challenging task given to Archimedes wherein he was asked to determine whether some silver was used in place of pure gold by an alleged dishonest goldsmith in preparation of a golden crown for King Hero II of Syracuse. The discovery of Archimedes principle revolves around a legendary "Eureka!" moment while taking a bath in a tub when he made this remarkable discovery about buoyancy. Even though the discovery of Archimedes principle was not directly linked with the BL, but it was an era when the interaction of a fluid with a solid surface was recognized and was considered as a possible thrust area of research in future.

Even though we did not see any rapid progress in the area of fluid dynamics, the importance of fluid characteristics and its pertinent nature were well-captured by the famous painter Leonardo da Vinci (1452 – 1519), who had drawn sketches of complex flows over objects in streams after a careful examination on the behaviour of fluids. At that time, nobody ever knew that his sketches would draw further attention of the scientists of new generations to come. The real milestone in the area of fluid dynamics can be attributed to Sir Issac Newton who devoted Book II of his Principia Mathematica (1687) exclusively to the examination of fluid dynamics and fluid statics in the

seventeenth century. He provided necessary momentum to the scientific community in understanding the nature of fluid flow through its mathematical formulation which took a precise shape during the century following the publication of Principia Mathematica (Anderson, 2005).

Our understanding of the nature of fluid flow witnessed considerable progress in the eighteenth century with impressive contributions of Daniel Bernoulli, Leonhard Euler, and Jean le Rond d'Alembert. One of the most important contributions of Bernoulli was in hydrodynamic, which appeared in 1738. His contribution "Hydrodynamica" contains a vast discussion on the principle of conservation of energy and the basic laws for the theory of gases and gave. Bernoulli and Euler dominated the mechanics of flexible and elastic body for many years and investigated the flow of fluids. They were interested to know about the relationship between the speed at which blood flows and its pressure. Euler made significant progress in the mathematical description of a fluid flow in terms of spatially varying 3-D pressure and velocity fields. His efforts led to modelling of the fluid flow as a continuous collection of infinitesimally small fluid elements. Even though Euler's contribution was of the discovery-class in theoretical fluid dynamics, he did not account for the effect of friction acting on the motion of the fluid, as he ignored viscosity in his equations. For a long period after the derivation of Eulers equations, all the theoretical developments related to the motion of fluids had considered them as media with perfect fluidity, or in other words devoid of viscosity, and equations of motion of fluids were limited to perfect fluids only. However, it was well-recognized for a long time that the friction of fluids was one of the main causes of the deviation of experiments from theory. Despite the importance of viscosity, only a few theoretical developments attempted to include its effects in the equation of motion of fluids.

Almost after a hundred years of Eulers equations, Claude-Louis Navier attempted to modify the Eulers equations to account for the effect of internal friction within a fluid flow in 1822. A few years later, this work was further extended by George Stokes in 1845 who was working on the pendulum experiments to show that viscosity could play a role on the altered behaviour of the ideal pendulum motion. Their efforts led to a system of nonlinear partial differential equations, now called the Navier-Stokes equations. The Navier-Stokes equation governs the motion of real viscous fluids and can be seen as Newton's second law of motion for fluids. In many practical applications in the area of fluid dynamics, we use solutions to the Navier-Stokes equation, but our theoretical understanding of the solutions to this equation is not well understood, primarily because of inclusion of turbulence, which is one of the greatest unsolved problems in physics. The importance of BL becomes pertinent here because this turbulence is one of the most inherent characteristics of BL that dominates the transport processes within the BL. Despite the immense importance of turbulence in fluid dynamics, a definite solution to the Navier-Stokes equations for practical flow problems remained a challenging task to the investigators who were working on the estimation of the frictional shear force on a surface immersed in a flow.

The inability to obtain a feasible solution of the Navier-Stokes equations became acute at the beginning of the 20th century when the Wright brothers were tirelessly working towards the calculation of the lift and drag on the first practical airplane. However, no invention waits for a comprehensive theoretical explanation for a long period. As and when the right time comes, the inventions take place in due course. This was perfectly true in the case of Wright brothers, who invented the first powered, sustained and controlled airplane flight on 17 December 1903. On one hand, the area of fluid dynamics was being explored for the practical applications in aerodynamics, the concept of BL, on the other hand, was still a mystery to many of the researchers at the beginning of 20th century. Under such background, Ludwig Prandtl, a humble and young German Professor presented a scientific paper titled "Uber Flussigkeitsbewegung bei sehr kleiner Reibung (English Translation: On the motion of fluids with very little friction)" at Third International Mathematical Congress at Heidelberg, Germany, on 8 August 1904 (Anderson, 2005; Eckert, 2017; Willert, 2019). In his 10 minutes long presentation, Prandtl proposed a new concept of the BL and showed that friction, however small, had to be taken into account in a thin layer along the solid wall. For the proposal of this new concept, Prandtl made use of a tank of about 1.5 m long with an intermediate bottom. The water in this tank was set in motion by a Paddle wheel and, after passing through a deflecting apparatus was allowed to enter the upper channel which was comparatively free from vortices. In his experimental setup, fine scales of micaceous iron ore were suspended in water so that the flow of the fluid can be captured through pictures. His entire experiment gave a brief account of boundary-layer theory, separation of boundary layer and delay of separation by suction. During those days, it was well-known that the inviscid flow equations would not be able to predict the drag experienced by bodies. Therefore, Prandtl argued that the fluid sticks to the surface of the body, in other words, the velocity of fluid remains zero on a stationary body or equal to the velocity of the body when the body is moving (Fig. 1). However, the velocity around the body which can be obtained by the inviscid flow theory would be outside a thin layer. In his seminal paper, Prandtl referred to this layer as a "transition layer", which was later accepted as the term "boundary layer".

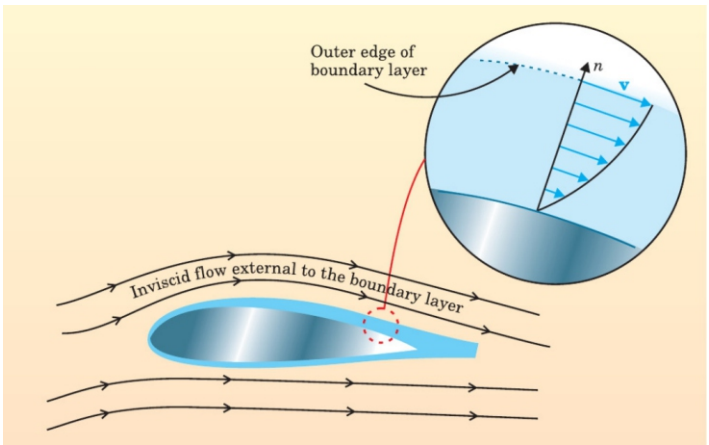

Figure 1. The concept of the boundary layer as proposed by Ludwig Prandtl in 1904. Here, a fluid flow can be viewed as comprising two parts. In a thin boundary layer adjacent to the surface, the effects of friction are dominant. Outside the boundary layer, flow is inviscid.

The concept of BL put forward by Prandtl was one of the revolutionary concepts for the futuristic world of aerodynamics and the modern world of fluid dynamics is still dominated by Prandtl's idea. Nonetheless, a formal discovery of a new concept of BL was archived in the symposium proceedings of Third International Mathematical Congress in 2005. The greatness of

this seminal paper was the humbleness of Ludwig Prandtl, who deserves full credit for the discovery of Boundary Layer, but he consistently used the word "Transition Layer" in his paper. The famous "Boundary Layer" term came into frequent usage later by Prandtl's students. Almost after 24 years of Prandtl's proposal of a new concept, the famous fluid dynamicist Sydney Goldstein asked Prandtl why his seminal paper was so short? Prandtl replied in a very humble manner that he was given only 10 minutes for his presentation, and he was under the impression that his paper could contain only what he had time to say. Prandtl's concept of BL remained unknown to many researchers for years and did not receive the recognition of what it deserved.

Unfortunately, the first half of the 20th century did not see significant and recognizable progress about the BL theory. It may also be worth pointing out that the global economy also had a serious setback due to World War - I and II which followed within a short span of period. Due to lack of funds for dedicated research and rivalry among the Axis Powers and Allies, the science was also attaining a kind of polarity with two front-runners: USSR and USA. During the Second World War in 1943, at the age of 25 years the famous Russian Physicist and Applied Mathematician A. M. Obukhov finished the remarkable paper titled "'Turbulentnost'v temperaturnoj - neodnorodnoj atmosfere (English translation: Turbulence in an Atmosphere with a Non-uniform Temperature)"(Obukhov, 1946). Because World War II ravaged around the globe at that time, his manuscript was not published until 1946. Unfortunately, it appeared in the very limited first issue of the Journal (Obukhov, 1946). Due to the lack of modern duplicating techniques, the paper was doomed to obscurity right from the start. Very few scientists outside the Soviet Union were aware of it, and even in the USSR, not many realized its real importance. In his paper, Obukhov introduced a "Length Scale (L)" of the dynamic turbulence sublayer. Obukhov proposed that the mean wind and temperature profiles must be determined by some universal function of the uniquely defined dimensionless height (L):

$$L = u_*^3 ./ \left(\kappa . \frac{g}{\theta_v} . \overline{w'\theta_v'} \right)$$

where, L is a characteristic scale for the thickness of the so-called 'dynamical sublayer', a layer where the influence of the stratification is negligible. The Length Scale (L) is connected with a dimensional analysis of the equation of turbulent kinetic energy (TKE) and the ratio of the buoyancy and shearing effects (Obukhov, 1951). With the introduction of a new length scale, it was also the first time when the contrasting features of BL for stable and unstable stratification were discussed scientifically. In this infamous paper, Obukhov postulated a parameter with the dimension of length, when used to scale the height above the ground z, yielded a dimensionless stability parameter, z/L, which can be expressed as the relative roles of shear and buoyancy in the production/consumption of TKE. This new revolutionary length scale was later named as "Obukhov Length" in his honour. Almost after a decade of introduction of 'Obukhov Length', A. S. Monin, one of the students of Obukhov extended this work and published mathematical formulation of BL theory entitled "Osnovnye zakonomernosti turbulentnogo peremeshivanija v prizemnom sloe atmosfery (English translation: Basic Laws of Turbulent Mixing in the Atmosphere Near the Ground)" in 1954, which has been recognized as the famous Monin-Obukhov (M-O) Similarity theory (Monin and Obukhov, 1954). It was an outcome of a fundamental experimental work at the Geophysical Main Observatory, Leningrad, in which Monin and Obukhov cited the famous work of Prandtl and also carried forward the concept of a zero-plane displacement (Monin and Obukhov, 1954).

Ever since, the proposal of M-O Similarity theory in 1954, the importance of ocean-land-atmosphere interaction has received a special attention with regard to the ABL processes. The area of atmospheric and oceanic modelling has now realized the importance of energy exchange at air-sea interface that forms a primary backbone of all the models dealing with the surface-layer turbulent exchange of momentum, heat, and moisture. Within a year of postulation of M-O Similarity theory, the famous British meteorologist Henry Charnock proposed a new constant for the estimation of wind stress on a water surface:

$$\frac{u}{u*} = \left(\frac{1}{\kappa}\right).log\left(\frac{gz}{u*^2}\right) + constant$$

This constant was introduced by Charnock in his famous one and half page discussion paper that appeared in Quarterly Journal of Royal Meteorological Society in 1955. The importance of scaling parameters for wind, temperature, and humidity were obviously becoming relevant to the meteorologists and oceanographers, particularly who were attempting to quantify the amount of air-sea interface fluxes of momentum, heat and moisture. In this area, due credit need to be paid to J. A. Businger, who put forward the mathematical formulation of turbulent transfer in atmospheric surface layer in 1971. Till date, the area of ocean-atmosphere interaction is dominated by the Businger (1971) equations which formulate the backbone of surface-layer parametrization schemes in atmospheric and oceanic models. After pivotal effort of Businger (1971), the role of air-sea exchange coefficients and their dependence on various important factors such as: roughness length for momentum, heat and moisture is well documented. We can also find numerous studies on the dependence of bulk transfer exchange coefficients on the stability functions, wind speed and various other factors.

Today, we have reasonable understanding about the air-sea interaction processes and their role in extreme weather events and energetics of atmosphere, it is equally important to respect and pay our homage to some of the top-class researchers in the past who could never receive the recognition which they deserved. Despite all the odds, their contributions are well appreciated, though it took years to accept their novel work. For example, Ludwing Prandtl must be credited for the discovery of boundary layer, but he never claimed to do so, and he retained all his description about this layer merely as a "Transition Layer". Today, we call this layer the famous "Boundary Layer". Extending the work in the area of boundary-layer theory, the classical work of Obukhov and Monin promised several new dimensions towards theoretical formulation of ABL processes, but they never sought any recognition of their work. It was years later, when their theory became the famous M-O Similarity theory. Almost in a similar line, we can not forget an impressive effort of Charnock, wherein he introduced a new constant for the estimation of wind stress over the water surface, and his work remained unnoticed for a few years. But on today's date, we call that constant as the "Charnock Constant" and his discussion paper is one of the most cited papers in the atmospheric sciences. Conclusively, the area of ABL and air-sea interaction processes are two strongly coupled fields, but

due to several reasons the duo had to suffer for slow progress in the past two centuries, but have finally been recognized as the primary thrust areas in the coupled ocean-atmosphere modelling.

References

Anderson, D. A., "Ludwig Prandtl's Boundary Layer", Physics Today, 42–48, 2005.
Businger, J. A., "Turbulent transfer in the atmospheric surface layer", Workshop on Micrometeorology, edited by: Haugen, D. A., American Meteorological Society, Boston, Mass, 67–100, 1973.
Charnock, H., "Wind Stress on a Water Surface", Quarterly Journal of Royal Meteorological Society, 1955.
Eckert, M., "Ludwig Prandtl and the growth of fluid mechanics in Germany", Comptes Rendus Mecanique, 345: 467-476, 2017.
Garratt, J. R., "The Atmospheric Boundary Layer, Cambridge University Press, Cambridge, 316 pp., 1992.
Monin, A. S., Obukhov, A. M., "Osnovnye zakonomernosti turbulentnogo peremeshivanija v prizemnom sloe atmosfery (Basic Laws of Turbulent Mixing in the Atmosphere Near the Ground)", Trudy geofiz. inst. AN SSSR 24(151), 163-187, 1954.
Obukhov, A. M., "Charakteristiki mikrostruktury vetra v prizemnom sloje atmosfery (Characteristics of the Micro-structure of the Wind in the Surface Layer of the Atmosphere)", Izv. AN SSSR, ser. Geofiz. 3, 49-68, 1951.
Obukhov, A. M., "Turbulentnost'v temperaturnoj - neodnorodnoj atmosfere (Turbulence in an Atmosphere with a Non-uniform Temperature)", Trudy Instituta Teoreticheskio Geofiziki AN SSSR 1, 95-115, 1946.
Stull, R. B., "An Introduction to Boundary Layer Meteorology", Kluwer Academic Publishers, Dordrecht, TheNetherlands, 666 pp, 1988.
Willert, C., Schulze, M., Waltenspül, S., Schanz, D., Kompenhans, J., "Prandtl's flow visualization film C1 revisited", 13th International Symposium on Particle Image Velocimetry – ISPIV 2019 Munich, Germany, July 22-24, 2019

Research Highlights

Impact of air-sea fluxes on the simulation of a tropical cyclone in the Bay of Bengal

* *Article based on Pant V., K. R. Prakash (2020), Response of air-sea fluxes and oceanic features to the coupling of ocean-atmosphere-wave during the passage of a tropical cyclone, Pure and Applied Geophysics, https://doi.org/10.1007/s00024-020-02441-z.*


Vimlesh Pant , Kumar Ravi Prakash
Centre for Atmospheric Sciences, Indian Institute of Technology Delhi, New Delhi

Tropical cyclone (TC) interacts dynamically and thermodynamically with the ocean through the heat, momentum, and moisture fluxes at the air-sea interface. Strong winds associated with the TC over the warm sea surface leads to enhanced evaporation rate and provides surplus latent heat flux conducive to sustain or intensify the TC. Strong wind stress produced by TC induces significant cooling on the ocean surface through enhanced entrainment at the mixed layer base, vertical mixing, and upwelling (Price, 1981; Price et al., 1994). The intensification of TCs is caused partly by the large air-sea fluxes of moisture and heat. However, an increase in surface roughness reduces wind speed that leads to a decrement of moisture flux (Chen et al., 2013). The columnar heat content of the upper ocean controls the air-sea interaction through modulating the sea surface temperature (SST), latent and sensible heat fluxes which, in turn, decides sustenance and intensity of TC (Shay et al., 2000). Numerical modeling studies based on uncoupled atmosphere (ocean) models utilize SST (winds) prescribed from observations or other stand-alone models. Therefore, any feedback between evolving surface properties on either side of the air-sea boundary is not considered in the uncoupled models. Coupled ocean-atmosphere models take into account the feedback through heat and momentum fluxes. Coupled models, therefore, can be used to understand the upper oceanic response to the TC passage (Prakash and Pant, 2017). Coupling of the wave model to the ocean-atmosphere coupled model provides an added advantage of 3-way feedback between ocean-atmosphere and wave environment. Incorporating effects of surface waves in the coupled model improves prediction of wind speeds, upper oceanic mixing, and fluxes of heat and momentum at the air-sea interface. Chen et al. (2013) showed that under the highly variable TC winds, the surface stress vector and local wind vector may not align which provides directionality component to surface roughness. Therefore, consideration of surface roughness as a scalar quantity in coupled wave models give rise to poor accuracy in simulations.

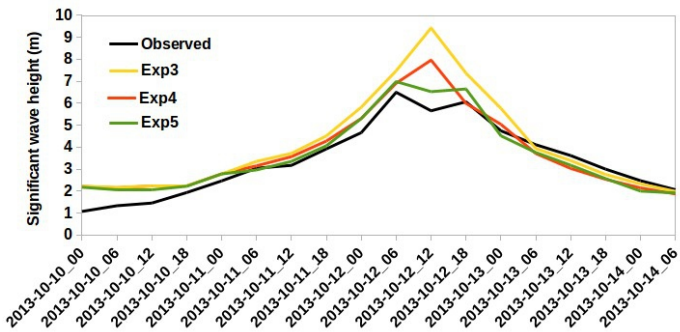

Figure 1: Comparison of simulated significant wave height (m) from the stand-alone SWAN i.e. Exp4 (red), WRF+SWAN i.e. Exp3 (yellow), and fully coupled model i.e. Exp5 (green) with that of observed (black) at the wave rider buoy location.

Different numerical experiments with uncoupled and coupled ocean-atmosphere-wave models were carried out for the case of TC Phailin in the Bay of Bengal

(BoB). TC Phailin, categorized as a very severe cyclonic storm (VSCS), was one of the strongest TC that occurred in the BoB. It originated in the
northern Andaman Sea on 7th October 2013 and intensified to severe cyclonic storm (SCS) on 10th October 2013. TC Phailin attained maximum wind speed of about 200 km h-1 at 0300 GMT on 11th October 2013 before it's landfall on 12th October 2013 near Gopalpur, Odisha. Further details of TC Phailin are described in IMD-report (2013). The differences among model experiments with different coupling options are analyzed to explain the impact of model coupling on the air-sea fluxes under the high wind conditions prevailing during the passage of TC Phailin over the BoB.

Model details

The 'Coupled Ocean Atmosphere Wave Sediment Transport' (COAWST) modeling system (Warner et al., 2010) has been used for our study. The COAWST modeling system used in this study includes atmospheric model 'Weather Research and Forecasting' (WRF-ARW), ocean model Regional Ocean Modelling System' (ROMS), and the spectral wave model 'SimulatingWAvesNearshore' (SWAN). To facilitate coupling between different modelling components, the 'Model Coupling Toolkit' (MCT) is used as a coupler in the COAWST modelling system. The domain of WRF, covering the BoB, set to be larger than the collocated domains of ROMS and SWAN models. The WRF model used a two-way nested domain with an outer fixed domain of 27 km resolution extending between 65–105° E and 1–34° N. The inner domain of 9 km resolution in WRF model moves with the translational movement of the cyclone.Exp1 used an uncoupled WRF-alone model. The coupled model experiments includeExp2 (WRF+ROMS), Exp3 (WRF+SWAN), Exp4 (SWAN-alone), Exp5 (WRF+ROMS+SWAN). Further details of model experiments for the study of air-sea fluxes are given in Pant and Prakash (2020).

Results

The uncoupled WRF-alone model in Exp1 found to have higher RMSE than the coupled models used in Exp2 and Exp5. The statistical error metrics clearly show an improvement in the wind speed in the fully coupled atmosphere-ocean-wave model (Exp5) as compared to atmosphere alone (Exp1) and atmosphere-ocean model (Exp2).Exp1 showed enhanced cooling over the entire domain with a cold bias up to -2 °C during the post-cyclone period. Coupled model configurations in Exp2 and Exp5 showed a better agreement with buoy temperature profiles whereas uncoupled model in Exp1 simulated shallower D23 and cold bias at the buoy BD10 location. While the significant wave height (Hs)of the order of 12 m were simulated by the uncoupled SWAN model in Exp4, it was about 10 m in case of fully coupled model in Exp5 on 12 October. However, Exp3 (WRF+SWAN) shows relatively higher Hs as compared to the fully coupled Exp5. Therefore, the coupled models reduces Hs by about 2-3 m as compared to the uncoupled SWAN model. The overestimation of the Hs peak-magnitude in Exp3 and Exp4 reduced in the fully coupled model (Exp5). Hence, Exp5 found to be in close agreement with the observed Hs values at the buoy location (Figure 1). The reduced Hs noticed in Exp5 was as a consequence of decreased surface wind stress when the information of surface waves from the SWAN model was routinely updated in the WRF model during the model integration. The surface drag coefficient and, therefore, bottom stress were found to be maximum in Exp1. The magnitude of bottom stress exceeded 2 Nm-2 in Exp1 that lead to the enhanced momentum transfer to the sea surface, and stronger surface currents in Exp1. In the

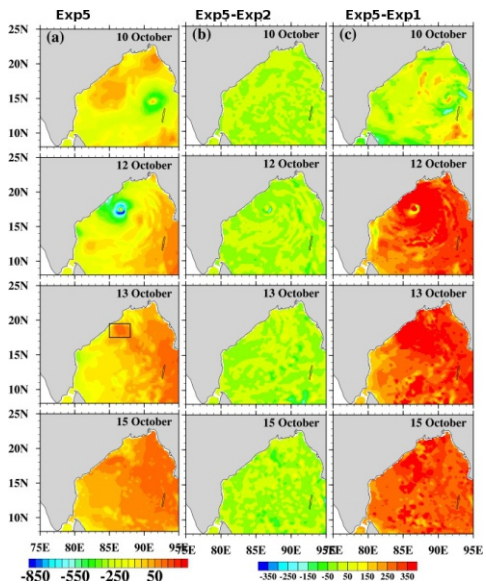

Figure 2: Net heat flux (Wm^{-2}) simulated from (a) Exp5 (b) difference between Exp5 and Exp2 (Exp5-Exp2) and (c) difference between Exp 5 and Exp1 (Exp5-Exp1).

presence of ocean surface waves in the coupled model in Exp5, the relative magnitude of bottom stress was higher than that of without including waves in Exp2 (WRF+ROMS). Coupling between the ocean-atmosphere models in Exp2 allows continuous feedback of SST simulated by the ocean model to the atmospheric model. Oceanic processes such as upwelling and mixing update SST in the ocean model that provides colder SST (in case of cyclone-induced upwelling) as the surface boundary condition to the atmospheric model and, thereby, reduces the surface wind stress and bottom stress in the coupled model experiment. In the case of oceanatmosphere-wave (Exp5) coupled model experiment, the wave amplitudes and associated crests and troughs of surface waves increase the roughness of sea surface. The enhanced surface roughness decreases the surface wind speed and increases bottom stress in the atmospheric model. As a result of the larger drag and bottom stress, the ocean surface stress was also higher in Exp5 than in other experiments. Therefore, the coupled model improved the near-surface simulations in the atmosphere and ocean through the surface drag and exchange effects (C and C), where C is a function of wind d k d speed through Charnock relationship, the exchange coefficient C is calculated using surface roughness length. C k d varies due to variations of wind speed during the cyclone and becomes more sensitive. Besides, wind-induced wave also offers higher Cd .

The net heat flux in uncoupled model (Exp1) reduced by a large amount as compared to the coupled model (Exp2 and Exp5) configurations (Figure 2). The impact of surface cooling due to loss of heat at the surface as highlighted by the negative heat flux (-500 to -800 W m-2) was localized in the vicinity of the cyclone in the coupled model experiments (Exp2 and Exp5). In contrast, the spatial extent and magnitude of heat loss on 12 October were found to be larger (about 300-400 W m-2 excess heat loss) in Exp1. Further, the negative net heat fluxes (-200 to -500 W m-2) persisted during the post-cyclone period (13-15 October) in Exp1. The mixed layer heat budget analysis showed that the contributions of the horizontal advection and net heat flux were dominating in case of the uncoupled model in Exp1. Whereas, in coupled models (Exp2 and Exp5), the reduced

magnitudes of net heat flux, advection, and residual terms lead to higher mixed layer heat storage than Exp1 on 12 October. The coupled model configuration provided periodic feedback of SST to the atmosphere that improved the heat fluxes in the atmospheric model in the coupled configuration. These results signify the importance of model coupling for a better simulation of SST by ocean model and heat fluxes by the atmospheric model.

References

Chen, S.S., Zhao, W.,Donelan, M.A.,Tolman, H.L. (2013), Directional wind–wave coupling in fully coupled atmosphere-wave-ocean models: Results from CBLAST-Hurricane, J. Atmos. Sci., 70, 3198–3215.

IMD-report (2013), Very severe cyclonic storm, PHAILIN over the Bay of Bengal (08–14 October 2013): a report. India Meteorological Department, Technical Report, October 2013.

Pant, V., Prakash, K.R. (2020), Response of air-sea fluxes and oceanic features to the coupling of ocean-atmosphere-wave during the passage of a tropical cyclone, Pure and Applied Geophysics.

Prakash, K. R., Pant, V. (2017) Upper oceanic response to tropical cyclone Phailin in the Bay of Bengal using a coupled ocean-atmosphere model, Ocean Dynamics, 67:51.

Price, J.F. (1981), Upper ocean response to a hurricane, J. Phys. Oceanogr., 11, 153–175.

Price, J.F., Sanford, T.B., Forristall, G.Z. (1994), Forced stage response to a moving hurricane, J. Phys. Oceanogr., 24, 233–260.

Shay, G., Goni, J., Black, P.G.(2000), Effects of a warm oceanic feature on Hurricane Opal, Mon.Weather Rev., 128, 1366–1383.

Warner, J.C., Armstrong, B., He, R., Zambon, J.B.(2010), Development of a coupled ocean atmosphere–wave–sediment transport (COAWST) modeling system, Ocean Model., 35:230244.

Research Highlights

Phytoplankton community structure in a contrasting physico-chemical regime along the eastern Arabian Sea during the winter monsoon

**Based on the following paper: Vijayan, A.K., Reddy, B.B., Sudheesh, V., Marathe, P.H., Nampoothiri, V.N., Harikrishnachari, N.V, Kavya, P., Gupta, G.V.M., Ramanamurthy, M.V. (2021) Phytoplankton community structure in a contrasting physico-chemical regime along the eastern Arabian Sea during the winter monsoon. Journal of Marine Systems, 215, https://doi.org/10.1016/j.jmarsys.2020.103501*

Vijayan, A.K., Reddy, B.B., Sudheesh, V., Marathe, P.H., Nampoothiri, V.N., Harikrishnachari, N.V., Gupta, G.V.M., Ramanamurthy, M.V.

The eastern Arabian Sea (EAS) basin is characterised by contrasting physical regimes during the winter monsoon (WM); a warm, oligotrophic waters makes the south EAS (SEAS) less productive when the convection-induced nutrient-rich condition enhances the phytoplankton production significantly in north EAS (NEAS). Moreover, the formation of high saline waters over the NEAS and the intrusion of Bay of Bengal (BoB) waters at the SEAS makes large salinity gradient across the EAS basin. The WM is also noted for subsurface chlorophyll maxima (SCM) in the SEAS while the phytoplankton communities are well distributed in the water column over the NEAS. Though there are a number of studies on physical dynamics of EAS, most of the biogeochemical and biological studies are confined to a regional, i.e., either NEAS or SEAS, and a basin-wide understanding is still lacking. The present study, carried out as part of the project *Marine Ecosystem Dynamics of eastern Arabian Sea* (MEDAS), is the first of its kind encompasses the entire eastern part of the Arabian Sea basin (between ~ 6-22°N and 77-67°E) with high-resolution sampling from coastal to offshore regions (Figure.1). The study highlights the differences in the distribution of phytoplankton community under contrasting warm, oligotrophic and cold, nutrient-rich south to north regimes along the EAS during WM.

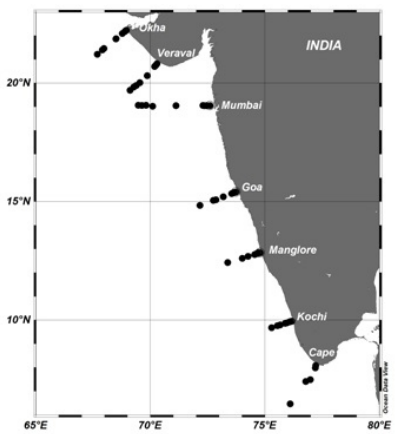

Figure 1: Sampling locations along the eastern Arabian Sea. The transects up to 15°N (Cape, Kochi, Mangalore, and Goa) are defined as southeastern Arabian Sea (SEAS) and the rest of transects (Mumbai, Veraval, and Okha) as northeastern Arabian Sea (NEAS). Each transect is sub-divided with respect to station depths as nearshore (10 to 30 m), shelf (40 to 100m) and offshore (1000 to 2000m).

The hydrographic conditions separated the surface EAS into two distinct regions during the WM - cold (23.3-26.9 °C), high-saline (35.2-36.4) waters in the NEAS and warm (27.4-28.4 °C), low-saline (32.6-35.5) waters in the SEAS (Table.1). The prevalence of cold high saline waters in the NEAS shows the signatures of convective mixing that were found prominent at the northernmost transect (Okha) and the signals were weaker towards the southern part of NEAS (Mumbai). The sea surface temperature (SST) was ~3-4ºC warmer in the SEAS than the NEAS. The warm (>28°C), low-saline (<34.5) layer in the offshore waters (upper 60 m) of the southern SEAS (Cape, ~7ºN) reveals the intrusion of Bay of Bengal (BoB) waters, which thinned towards the north and was restricted to the upper ~10 m of the water column at ~15º N (Goa).The coastal waters were well-mixed throughout the EAS with distinct characteristics in the NEAS and SEAS. While BoB waters (S<34.5) influenced the coastal waters of the SEAS (up to ~15° N), the Arabian Sea High Saline Water mass (S>35.3) occupied coastal waters of the NEAS.

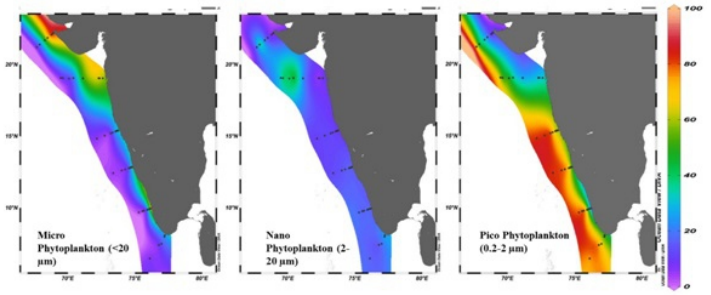

Figure 2: Percentage distribution of Phytoplankton size fractionsin the surface waters of eastern Arabian Sea .

The contribution of major phytoplankton groups to total chlorophyll a was calculated using CHEMTAX software as detailed in Roy et al. (2015).The statistical analyses was carried out using PRIMER® ver. 6 (Warwick and Clarke et al. 2005).Different phytoplankton size fractions showed distinct spatial heterogeneity in their distribution in the coastal and offshore regions of the EAS (Figure.2). Both NEAS and SEAS showed significant variations in terms of basin-scale column integrated chlorophyll *a* (Chl*a*) concentration in the upper 100m (Figure.3), it was higher in the NEAS (16 to 118 mg m^{-2}) relative to SEAS (9 to 79 mg m^{-2}). The chromatographic analysis revealed the dominance of diatoms, as inferred from the increased concentration of fucoxanthin, in the nearshore and shelf regions (Figure.4). Large phytoplankton (diatoms) dominated the coastal regions, indicating an herbivorous control in the food chain. Diatom abundance was found to be controlled by nutrient availability and was higher in the NEAS nearshore waters. The offshore waters are characterised by large proportions of pico-nano plankton along with considerable micro phytoplankton (Figure 2). Both physical and chemical conditions chiefly controlled the offshore phytoplankton population during the WM. The statistical analysis showed that it was the high silicate concentration (9.5±6.8 µM) in the nearshore waters of the NEAS and high Si/N ratio (4.4±3.4) in the nearshore waters of the SEAS that played a major role in regulating the abundant diatom population. At the same time, temperature and salinity together with nutrients structured the offshore phytoplankton assemblages during WM. The nutrient chemistry of the offshore regions revealed that entrainment of sub-halocline nutrients into the sunlit water column through convective mixing supported the dominant cyanobacterial population in the NEAS. In the warm oligotrophic waters of the SEAS, the substantially high NH_4^+ concentration (1.3±0.5µM) indicates that the regenerated production sustained the dominant prochlorophytes. The large proportion of pico-nanoplankton in the offshore of EAS suggests a transition of the ecosystem to a mixotrophic condition where micro-fractionof phytoplankton continued to contribute to the total phytoplankton biomass. Whereas the dominance of large phytoplankton like diatoms indicates herbivorous control in the food chain in the coastal regions.

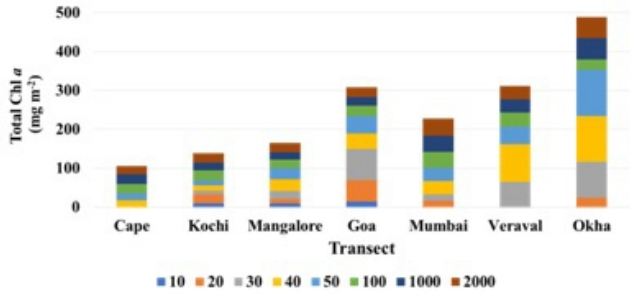

Figure 3: Column integrated chl a(mg m^{-2}) across all the transects/stations along the eastern Arabian Sea during winter monsoon.

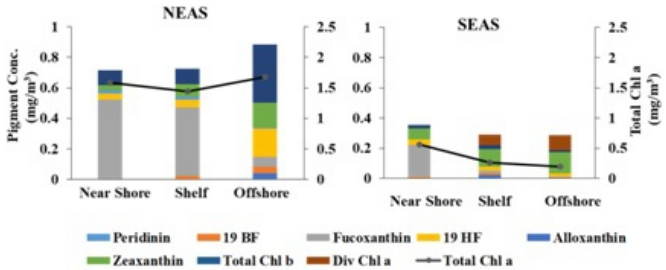

Figure 4: Surface Phytoplankton pigment distribution along the eastern Arabian sea.

References

Jeffrey, S.W., Mantoura, R.F.C., Wright, S.W. (Eds.), 1997. Phytoplankton Pigments in Oceanography. UNESCO Publishing, Paris. 661p.

Jeffrey, S.W., Vesk M., 1997. Introduction to marine phytoplankton and their pigment signatures, In: Phytoplankton pigments in oceanography: guidelines to modern methods, S.W. Jeffrey, R.F.C. Mantoura and S.W. Wright (eds.), UNESCO Publ., Paris, 37-84.

Jeffrey, S. W., Wright, S. W., 1997. Qualitative and quantitative HPLC analysis of SCOR reference algal cultures. In "Phytoplankton Pigments in Oceanography: Guidelines to Modern Methods". (Eds. S. W. Jeffrey, R. F.C. Mantoura and S. W. Wright.) pp. 343-360. (UNESCO: Paris.).

Legendre, L., Demers, S., 1984.Towards dynamic biological oceanography and limnology, Can.J.Fish.Aquat.Sci., 41, 2-19.

Legendre, L., Rassoulzadegan, F., 1995.Plankton and nutrient dynamics in coastal waters, Ophelia. 41, 153-172.

Mackey, M.D., Mackey, D.J., Higgins, H.W., Wright, S.W., 1996. CHEMTA—a program forestimating class abundances from chemical markers: application to HPLC measurements of phytoplankton. Mar. Ecol. Prog. Ser. 144, 265–283.

Roy, R., Chitari, E., Kulkarni, V., 2015. CHEMTAX-derived phytoplankton community structure associated with temperature fronts in the northeastern Arabian Sea. J. Mar.Syst. 144, 81–91.

Warwick, R., Clarke, K., 2006. PRIMER 6. PRIMER-E Ltd, Plymouth, pp. 615.

Wright, S.W., van den Enden, R.L., Pearce, I., Davidson, A.T., Scott, F.J., Westwood, K.J.,2010. Phytoplankton community structure and stocks in the Southern Ocean(30–80 E) determined by CHEMTAX analysis of HPLC pigment signatures. Deep-Sea Res. II. 57, 758-778.

OSI Webinar Series (April – May – June, 2021)

OSI Webinar - April 2021
Date: 22 April, 2021, Time: 16:00-17:00 IST
Speaker: Dr. V.S.N. Murty, CSIR-Emeritus Scientist and Chief Scientist (Retd.), NIO
YouTube Link: https://youtu.be/VZ8W8PAOZps
Topic: SMAP Sea Surface Salinity variability at intra-seasonal and synoptic scales in the North Indian Ocean and their impact on the Southwest Monsoon

About the Talk: Analysis of Soil Moisture Active Passive (SMAP) mission derived SSS during April 2015 to December 2017 in the Bay of Bengal (BoB) and its further analysis with other data sets during the Southwest Monsoon (SWM) period of 2020 (1 June – 17 August) in the Southeastern Arabian Sea (SEAS) reveals the i) existence of 30- to 90-day and 10- to 20-day period Intraseasonal Oscillations (ISO) and 3-7- day Synoptic Oscillations (SO) in SSS during the SWM and Fall seasons, and ii) occurrence of peak SO in moisture flux and upper layer Ocean Heat Content in the SEAS, 1-2 days prior to the monsoon onset over Kerala. The seasonal SMAP SSS anomaly (SSSA) minimum (-0.5 to -1.0) occurs in October in the northern BoB, wherein the 30- to 90-day ISO has larger amplitude (-0.2 to 0.35 psu). This ISO leads SST and then follows precipitation augmenting (suppressing) precipitation as part of active (break) phase of SWM.

In the month of May 2021:
Indian Ocean Blue Economy Summit – Webinar on Blue Economy in the Indian Ocean region towards United Nations Decade of Ocean Science for Sustainability (2021-2030) was held on May 6, 2021 (8:30 AM – 12:30 PM UTC).

This event was jointly organized by the IOC Regional Committee for the Central Indian Ocean (IOCINDIO), IEEE Oceanic Engineering Society, Marine Technology Society (MTS), Ocean Society of India (OSI), Kuwait Institute for Scientific Research (KISR), Kuwait, Ministry of foreign Affairs, Bangladesh, South Asia Cooperative Environment Programme (SACEP), Department of Oceanography, University of Chittagong, Bangladesh, Indian Institute of Technology, Madras, India, Basrah Marine Science Centre, Iraq, Iranian National Institute for Oceanography and Atmospheric Science, Iran, Ministry of Municipality and Environment, State of Qatar, National Institute of Oceanography, Pakistan, University of Portsmouth, UK and King Abdullah University of Science and Technology, Saudi Arabia.

The inaugural talk was delivered by Prof. Peter Haugen, Former Chair, IOC, Programme Director at Institute of Marine Research, Norway and Professor at University of Bergen, Norway. The title of talk was 'Towards sustainable ocean economy and ecosystem-based ocean management in Norway'. This talk covered the vision for clean and rich oceans and coastal regions. Three oceanic areas viz; the North Sea, the Norwegian Sea, and the Barents Sea off Lofoten were chosen for integrated ocean management and marine spatial planning in Norway that involves countries and municipalities. Interesting examples on Salmon farming highlighting on the crucial role of environmental regulation and management were discussed. Further, Salmon lice monitoring using traps/gill nets, sentinel cages, trawling, and modeling aspects in the wild since 2010 were highlighted. Importance of traffic light system in regulating the level of salmon lice induced mortality on wild salmonids at production areas with risk levels of mortality was demonstrated. The talk also highlighted on the role of ocean panel in climate-based solutions, along with ocean-based climate mitigation measures prone to have more benefits than trade-offs. The importance of sustainable planning along with the commitment of ocean panel providing effective protection, sustainable production, and equitable prosperity have been highlighted in the talk.

This event was chaired by Mr. Rear Admiral (Retd.) Khurshid Alam, Bangladesh and co-chaired by Dr. M. A. Atmanand, Chair IOCINDIO, India. The other distinguished members in the Organizing Committee were: Dr. Kawser Ahmed, Bangladesh; Dr. Md. Salimullah, Bangladesh; Dr. Marie-Alexandrine Sicre, France; Dr. M. Ravichandran, India; Dr. Srinivas Kumar, India; Dr. Prashant Srivastava, India; Dr. SajaFakherldine, Kuwait; Dr. Abtahi, Iran; Dr. Ali Bassal Mahmood, Iraq; Dr. Gilbert Siko, South Africa; Dr. Aruranthan, Sri Lanka; Dr. Alan Evans, U.K; Dr. Juma Al-Muskati, Oman; Dr. Samina Kidwai, Pakistan; Dr. Wong, Qatar; Dr. Margareth S. Kyewalyanga, Tanzania; Dr. M.Ashraf Haidari, South Asia Cooperative Environment Programme (SACEP), Srilanka; and Dr. YasserAbualnaja, KAUST, Saudi Arabia.

OSI Webinar - June 2021
Date: 28 June, 2021, Time: 11:30 - 12:30 IST
Speaker: Prof. Naresh K. Vissa, Asst. Professor, NIT Rourkela
YouTube Link:
https://youtu.be/1NV1b4g3xX8
Topic: Tropical Ocean and Atmosphere Interactions

About the Talk: In the tropics, oceanic and atmospheric coupled systems occur at various spatial and temporal scales such as interannual (e.g. ENSO, IOD), intraseasonal (e.g. MJO, BSISO), quasi-biweekly (e.g. Equatorial Waves) and synoptic (e.g. Tropical cyclones, depressions). Observed features of the coupled systems are revealed from in-situ and satellite measurements, structure and movement of these systems will be discussed. Various mechanisms have been proposed to understand the genesis, mature and dissipation of these coupled systems. In this talk we will primarily focus on the mechanisms that are related to ENSO and MJO. Role and importance of air-sea interactions for the sustenance of these coupled systems will be presented. Finally, as a case study how these air-sea fluxes are represented in the CMIP models will be discussed for boreal summer intraseasonal oscillations over the North Indian Ocean.

Articles/research highlights of general interest to the oceanographic community are invited for the next issue of the Ocean Digest. Contributions may be emailed to **osioceandigest@gmail.com**

Cover Photo: *Protoreaster linkii* at Angria Bank